Noyaux exotiques : Haloes

N.A. Orr

Noyaux Exotiques: Haloes

Nigel Orr,
Laboratoire de Physique Corpusculaire,
IN2P3 - CNRS, ISMRA et Université de Caen,
14050 Caen Cedex, France

Resumé

Un bref aperçu du halo nucléaire est presenté. Après quelques rappels historiques les caractéristiques générales des halos sont discutées dans le cadre d'un modèle simple. Les conditions gouvernant la formation des halos sont explorées, ainsi que deux sujets d'intérêts actuels: les résonances à basse énergie et les correlations entre les nucleons du halo.

Abstract

A brief overview of the nuclear halo is presented. Following some historical remarks the general characteristics of halo systems are discussed with reference to a simple model. The conditions governing the formation of haloes are also explored, as are two subjects of current interest — low-lying resonances and halo nucleon correlations.

I Introduction

The size and distribution of matter in the nucleus are fundamental questions in nuclear physics. Indeed, historically such studies may be traced back to Rutherford and Chadwick who derived the first estimates of nuclear sizes from deviations in the scattering of alpha particles from pure Coulomb scattering. Subsequent experiments demonstrated that to first order the nucleus could be represented as a sphere of constant density whereby the radius is,

$$R = r_o A^{1/3} \; ; \; r_o \approx 1.2 fm \tag{1}$$

In more recent times high energy electron scattering has been used in a similar manner to probe in detail the spatial distribution of the nucleus [1]. Such studies, as indicated in figure 1, demonstrated that the nuclear surface is diffuse. By combining electron scattering, which is sensitive to the charged matter distribution, with high energy hadron scattering differences in the neutron and proton matter distributions may be probed. For light nuclei the proton and neutron density distributions have been found to be essentially identical. For heavy nuclei differences appear as a result of the increasing N/Z ratio (1.54 for ^{208}Pb); the central neutron density becomes higher than that of the protons and a small difference

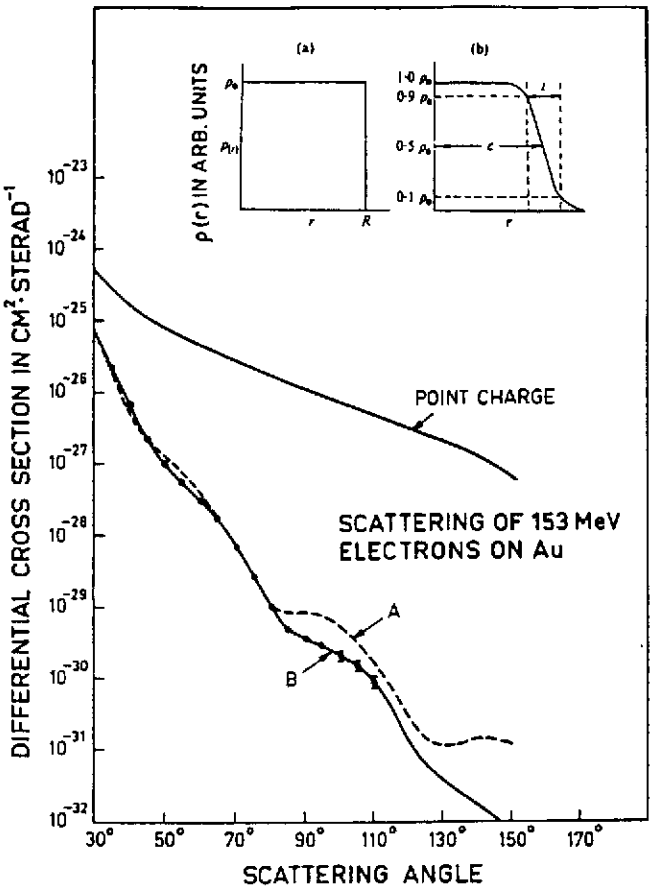

Figure 1: Angular distributions for e^--scattering on Au for various (charge) density distributions [2]: (A) $\rho(r) = \rho_0$ for $r < R$; and (B) the Fermi distribution, $\rho(r) = \rho_0/[1+e^{(r-c/a)}]$, where the surface diffusness is defined by $t = 4.39a$. $< r^2 >= \frac{3}{5}(c^2 + \frac{7}{3}\pi^2 a^2)$ and $< r^2 >^{1/2} < c < R$ with $R^2 = c^2 + \frac{7}{3}\pi^2 a^2$. For Au, $R = 6.87$fm (equation 1); $c = 6.38$fm and $a = 0.53$fm.

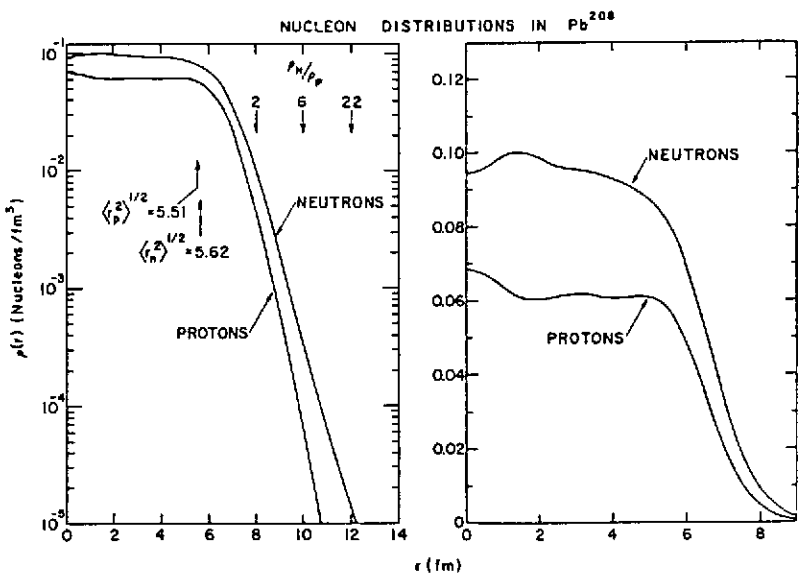

Figure 2: Calculated proton and neutron densities in ^{208}Pb [4].

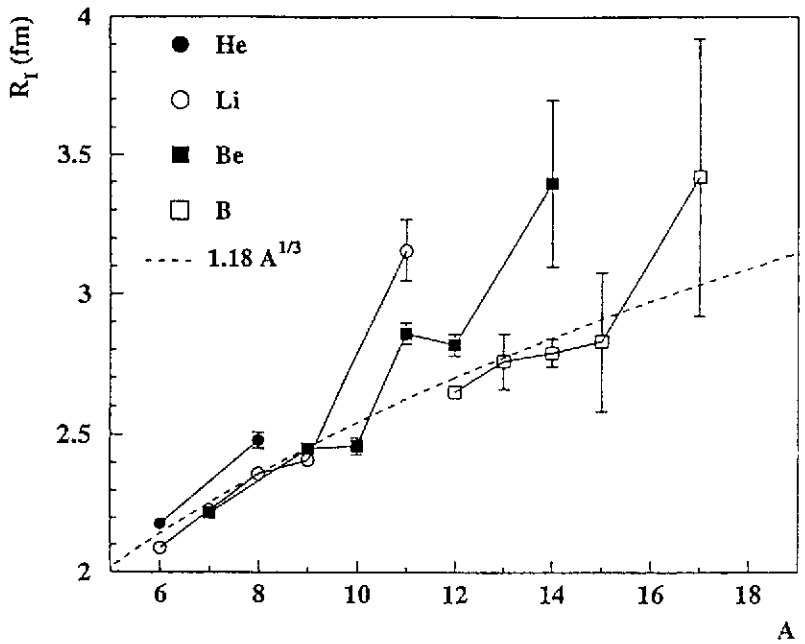

Figure 3: Interaction radii derived from high energy total interaction cross section measurements [6].

(~0.1 — 0.2 fm) develops between the neutron and proton RMS radii (figure 2), an effect first predicted by Johnson and Teller [3].

The most extreme neutron-to-proton ratios ($N/Z \leq 3$) are found at the driplines for the very light nuclei. Nuclei lying at the limits of particle stability are by definition weakly bound[1], a feature which as will be seen is central to the formation of haloes. Experimentally, the conventional probes discussed above cannot be employed for nuclei far from stability due to the short halflives and very low production yields [5] . Instead relatively high cross section processes employing beams of the nuclei of interest must be used.

Pioneering experiments of this kind, in which the total interaction cross sections (σ_I) for a variety of very light, neutron-rich nuclei were measured, were carried out in the mid-1980's at the BEVELAC using a simple transmission method [6]. These measurements indicated that ^{11}Li (S_{2n}=0.3 MeV), ^{11,14}Be (S_n=0.5 MeV, S_{2n}=1.3 MeV) and to a lesser extent ^{6,8}He exhibit much larger cross sections than expected on the basis of the systematics for the neighbouring isotopes. In simple terms the interaction cross sections obtained for light targets may be used to derive an effective interaction radius,

$$\sigma_I = \pi[R_I(proj) + R_I(target)]^2 \qquad (2)$$

The projectile and the large cross sections were thus interpreted[2] as reflecting abnormally large matter radii (figure 3).

[1]Typically by less than 1 MeV for the last nucleon(s) as opposed to stable nuclei where the binding energy is ~8 MeV/nucleon.

[2]Following the measurement of the spin and magnetic moment of ^{11}Li [7] which excluded a large deformation as the origin of the enhanced cross section.

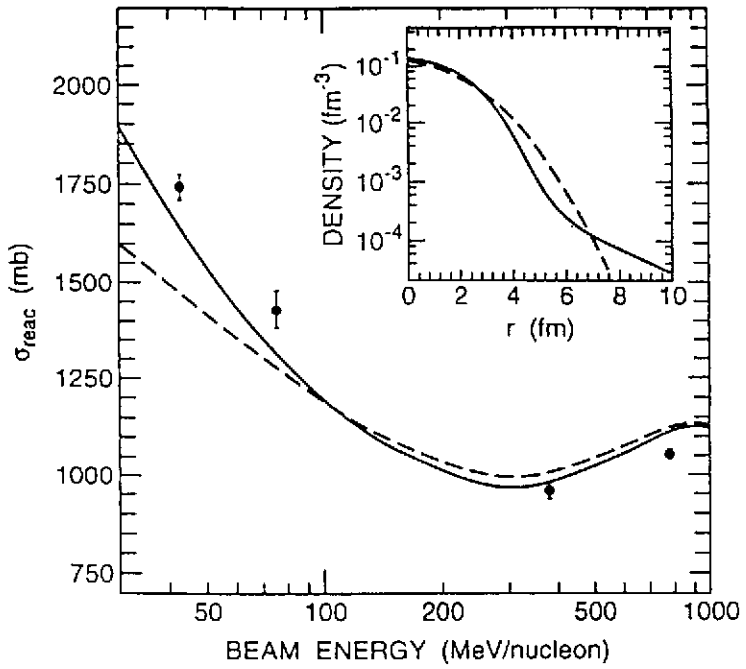

Figure 4: Total reaction cross sections for ^{11}Li on a carbon target compared to Glauber model calculations for density distributions with (solid line) and without (dashed line) a halo [12].

The very weak binding of the valence neutrons in these systems suggests that it is these nucleons which are responsible for the increased sizes. The observation of a constant charge changing cross section along an isotopic chain [8] and the separability of the total interaction cross sections [9],

$$\sigma_I(A) \;=\; \sigma_I(A - halo) + \sigma(A)_{-halo} \tag{3}$$

support a model in which a "core" $(A - halo)$, resembling a normal nucleus, is surrounded by an extended, "halo"[3], distribution formed by the valence neutrons.

As reactions at different energies probe different distance scales it has proven possible to map the density distribution of halo systems. In particular, by combining measurements of total reaction cross sections[4] with a reaction theory such as that of Glauber, which incorporates projectile and target density distributions[5], the form of the halo has been established as a long, low density tail (figure 4).

[3]A term which was first coined in reference to the much smaller effects observed in heavy, stable nuclei (figure 2) [4]. Unfortunately, while the physical origins are different in the two cases the same term has been retained.

[4]With the recent advent of relatively intense beams of halo nuclei at very high energies, it is now becoming possible to utilise standard methods, such as proton scattering [10].

[5]As pointed out by Al-Khalili and Tostevin [11], the few-body structure (core + halo nucleon[s]) of halo nuclei should be explicitly taken into account. The resulting increased transparency leads to significant increases in the estimated matter radii with respect to the initial analyses of the total interaction cross section data [6].

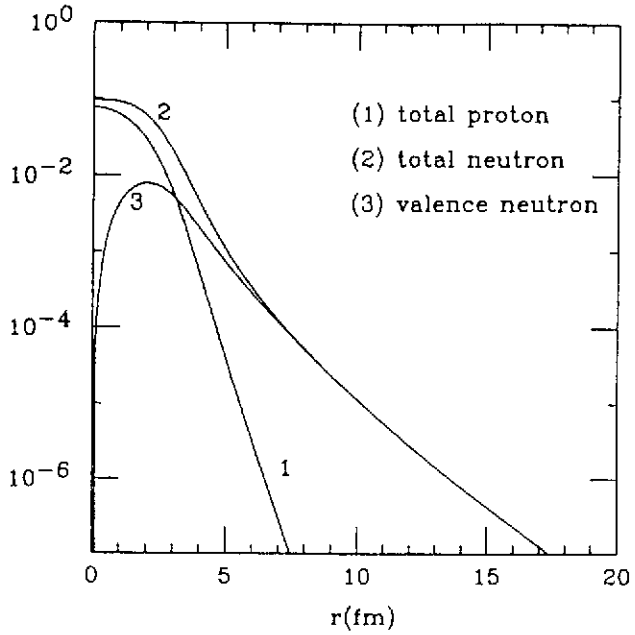

Figure 5: Density distribution for ^{11}Li calculated using the Hartree-Fock model and shell model occupation probabilities [13].

II General Properties

Having arrived at an image of the halo (figure 5), some of the physical features may be examined. To do so it is illustrative to introduce the simple quasi-deuteron model which was first applied to ^{11}Li in a seminal paper by Hansen and Jonson [14]. As the name suggests, the model was developed by analogy with the deuteron, a relatively weakly bound (E_B = 2.2 MeV) and extended ($< r^2 >^{1/2} \simeq$ 2.2 fm) system. Assuming a square well core potential of radius R in which the neutron is bound by B, the external solution to the Schrödinger equation is a Yukawa wavefunction of the form [14],

$$\psi(r) \;=\; \sqrt{2\pi\kappa}\;\frac{exp\;(-r/\kappa)}{r}\;\frac{e^{\chi}}{(1+\chi)^{1/2}} \tag{4}$$

characterised by a decay length,

$$\kappa \;=\; \hbar/\sqrt{2\mu B}$$

where: $\mu = A_h.A_c/(A_h + A_c) = A_h.A_c/A$ is the reduced mass; A, A_c and A_h the masses of the nucleus, core and halo respectively; and $\chi = R/\kappa$.

It should be noted that a number of assumtions are implicit in the model. Firstly the core and halo are treated as inert objects with the latter considered as a dineutron in the case of a two-neutron halo such as ^{11}Li. Secondly the halo neutron is assumed to have an angular momentum of zero (s-state) with respect to the core.

The mean square radius is defined, in terms of the matter density distribution, $\rho(r)$, as,

$$< r^2 > = \frac{\int \rho(r) r^4\, dr}{\int \rho(r) r^2\, dr} \tag{5}$$

Thus, for $\kappa > R$,

$$< r_{halo}^2 > \approx \frac{\kappa^2}{2}\frac{(1+2\chi)}{(1+\chi)} \tag{6}$$

and,

$$< r_{halo}^2 >^{1/2} \sim \frac{\kappa}{\sqrt{2}} = \frac{\hbar}{2\sqrt{\mu B}} \tag{7}$$

Clearly then, as the binding energy decreases to zero the size of the halo diverges rapidly (figure 6, Table 1). Conversely, in the limit of large binding the halo vanishes. The halo may thus be regarded as a threshold effect whereby the loosely bound valence nucleon(s) tunnels with significant probability into the (classically forbidden) region outside the potential well. Haloes are thus expected to be confined to only the most weakly bound of states.

As the size depends inversely on the reduced mass, for the same mass and binding the halo will be more pronounced for a two-neutron halo. Furthermore, the influence on the size of the nucleus diminishes with the overall mass of the system,

$$< r_m^2 > = \frac{A_c}{A} < r_c^2 > + \frac{\mu}{A} < r_h^2 > \tag{8}$$

A	B [MeV]	κ	$< r_h^2 >^{1/2}$ a) [fm]	$< r_m^2 >^{1/2}$ b) [fm]	$\delta < r^2 >^{1/2}$ c) [fm]	Γ [MeV/c]
11	0.1	15.2	11.5	4.1	1.5	26
	0.5	6.8	5.4	2.9	0.33	58
	1.0	4.8	3.9	2.7	0.13	82
21	0.1	14.8	11.4	4.0	0.74	27
	0.5	6.6	5.4	3.4	0.12	60
	1.0	4.7	3.9	3.3	0.03	84

a) Equation 6.

b) Equation 8, with $R_{10} = 2.60$ fm, $R_{20} = 3.25$ fm (equation 1).

c) $< r_h^2 >^{1/2} - < r_m^2 >^{1/2}$

Table 1: Quasi-deuteron model description of A=11 and 21 one-neutron halo systems.

A spatially extended distribution such as the halo is characterised, via the Uncertainty Principle, by a narrow distribution in momentum of the halo neutron(s) — typically some 4-5 times narrower than that of nucleons in normal nuclei ($p_{Fermi} \approx 225$ MeV/c). Furthermore, the distribution in momentum is directly related to the spatial wavefunction via the square of the Fourier transform. Thus the intrinsic momentum content of the halo, if experimentally accessible, could provide a powerful probe of the halo [15].

In the case of a Yukawa, the momentum density distribution is Lorentzian in form,

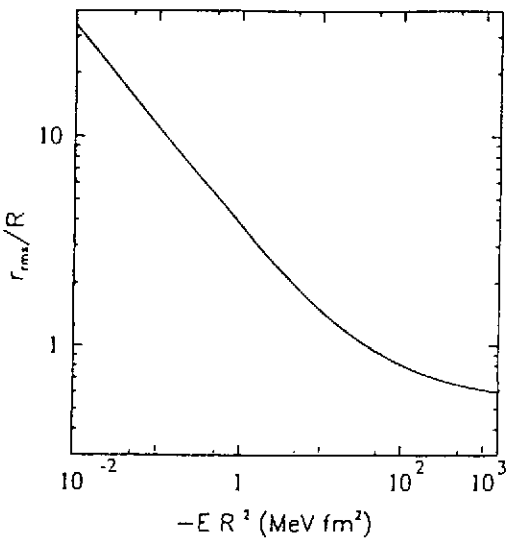

Figure 6: RMS halo radius as a function of binding energy, E (adapted from ref. [26]).

$$w(\mathrm{p}) \;=\; |\psi(\mathrm{p})^2| \;=\; \frac{\Gamma}{2\pi^2}\,\frac{1}{\left(\frac{\Gamma^2}{4}+\mathrm{p}^2\right)^2} \tag{9}$$

characterised by,

$$\Gamma \;=\; 2\hbar/\kappa$$

Despite the simplicity of the model described here, it does provide a reasonable description of the neutron halo. Indeed, the asymptotic behaviour of wavefunctions resulting from more realistic models is typically the exponential decay of a Yukawa. In the case of ^{11}Be, the physical basis of such a description is reasonably well founded as the single valence neutron is bound by only 500 keV and occupies a predominately $2s_{1/2}$ configuration. The predicted $< r_m^2 >^{1/2}$ of 2.9 fm (Table 1) is in good accord with that derived from total interaction cross section measurements [6, 11].

Turning to the momenta, a distribution characterised by $\Gamma_{intrinsic}$ = 58 MeV/c is predicted (Table 1). In the simplest approach, the momentum distributions of the fragments — charged core or neutrons — from high energy dissociation reactions on light targets (i.e., nuclear breakup) are assumed to measure directly the internal, or intrinsic, momentum distribution; the so-called Serber or "Sudden Approximation"[6] [19]. As typically a single momentum component (parallel or transverse to the beam direction) is measured in an experiment, the measured distribution is modified[7] from the three dimensional distribution. For example, in the case of a measurement of the distribution parallel to the beam (z) axis using a device with transverse acceptances much larger than the characteristic width of the distribution,

[6] A model developed, once again, for the deuteron.

[7] It has been suggested that for absorption (and diffraction), the wavefunction is essentially factorised in the reaction process [16]. The experimental acceptances would thus not influence the lineshape of the distribution.

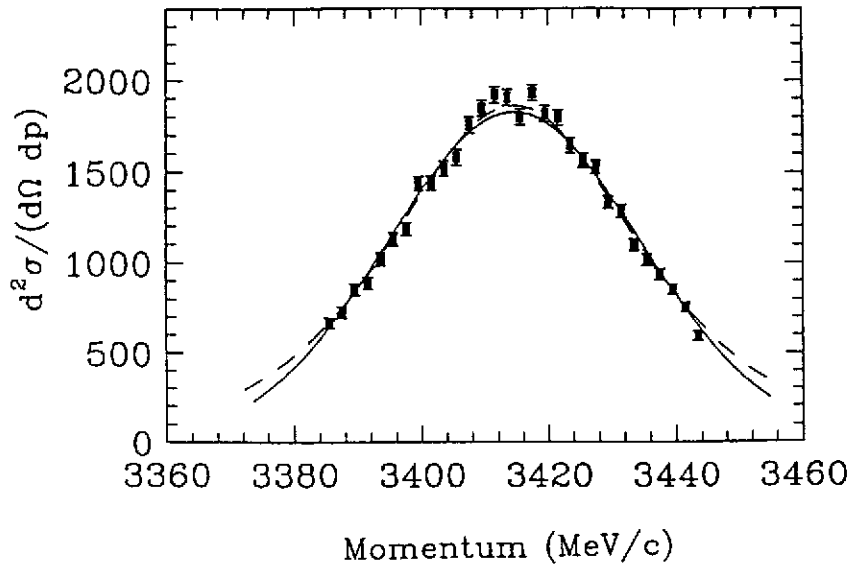

Figure 7: Longitudinal momentum distribution for ^{10}Be fragments following the breakup of a 63 MeV/nucleon ^{11}Be beam on a Be target [20].

$$w(p_z) = \int_{p_x}\int_{p_y} w(\mathrm{p})\, dp_x dp_y \tag{10}$$

Which, in the case of the Lorentzian results in a measured distribution of the form,

$$\frac{d\sigma}{dp_z} = \frac{\Gamma}{2\pi}\frac{1}{\left(\frac{\Gamma^2}{4}+p_z^2\right)^2} \tag{11}$$

where,

$$FWHM = \Gamma$$

Experimentally, the longitudinal momentum distributions for ^{10}Be fragments from the breakup of ^{11}Be exhibit widths of 42$\pm$2 MeV/c [20] (figure 7), in reasonable agreement with the $\Gamma_{intrinsic}$ derived fom the simple quasi-deuteron model (Table 1). While space does not permit a detailed discussion of fragment momentum distributions and the relationship to the intrinsic halo neutron distributions [15], it should be stressed that the simple picture presented above is in reality complicated by a number of factors. In particular, the perturbing effects of the reaction process and final state interactions (FSI) in the exit channels play roles in defining the final measured fragment momentum distribution.

In the case of FSI, the effects are most pronounced on the neutron distributions[8] from the breakup of two-neutron halo nuclei, whereby breakup may proceed via resonances in the unbound $A-1$ systems (eg., ^{10}Li in the case of ^{11}Li). As to the reaction, this will be governed by the nuclear interaction for light targets and a mixture of Coulomb and nuclear for heavy targets. For well developed halo systems the Coulomb breakup dominates, as illustrated in figure 8 [21]. In this example the heavy target reaction data is very forward

[8]Owing to the much smaller mass than that of the core fragment.

peaked and is well reproduced assuming Coulomb breakup. The light target data exhibits a broad distribution characteristic of diffractive dissociation — nuclear dissociation being composed of diffractive and absorptive components, typically of equal probability [16, 22].

Importantly the reaction process defines the impact parameter range for the collision, thus providing addition bias to the observed momentum distributions. In particular, the core fragment distributions for breakup on a light target — long assumed for measurements made parallel to the beam direction to provide the most direct measure of the intrinsic distributions — are limited to probing only radii greater than that of the core [15, 16, 17][9]. This results in distributions narrower than the intrinsic momentum distributions; an effect that will be in general more pronounced for the less well developed haloes.

As alluded to above, another distinguishing feature of halo nuclei is a large Coulomb (or electromagnetic — EMD) dissociation cross section for the channel core + neutron(s). Given the very weak binding of the neutrons to the core, such an effect is not suprising as the (charged) core is easily separated in the Coulomb field of the target from the (uncharged) neutrons. As summarized in figure 9, the EMD cross section increases rapidly with decreasing binding of the valence neutrons and with decreasing beam energy, E. In the simple quasi-deuteron model [14],

$$\sigma_{EMD} \sim \frac{Z^2_{target} Z^2_{proj}}{E.B} \tag{12}$$

Before closing this section, it should be stressed that the quasi-deuteron model has been discussed primarily for illustrative purposes. Indeed, even in the case of ^{11}Be it represents an approximation, albeit a reasonable one. Clearly the next step in a more complete description would employ a $2s_{1/2}$ neutron bound in a more realistic potential, such as a Woods-Saxon [16, 17]. Even then, the well known deformed nature of ^{10,11}Be, and consequent mixing of higher l configurations would be ignored [23].

III Conditions Governing Formation

As seen in the preceeding section, in a simple picture the development of a halo is governed by the binding energy of the valence neutron(s) and the mass of the system. The configuration occupied by the valence neutron(s) will also influence the spatial extent of the wavefunction. In particular, neutrons in states of non-zero orbital angular momentum, l, will encounter a centrifugal barrier,

$$V(r) = \frac{l(l+1)\hbar}{2mr^2} \tag{13}$$

As a consequence, the spatial extent of the wavefunction will be increasing limited with increasing l. The results for a single neutron bound in a square well potential ($A_c = 10$) for nonzero angular momenta are displayed in figure 10. Clearly for $l = 0$ and 1 the size of the system diverges as the binding energy approaches zero, while being confined for $l = 2$. The

[9] A strong absorption limit forseen in the by Hüfner and Nemes [18] and Serber [19].

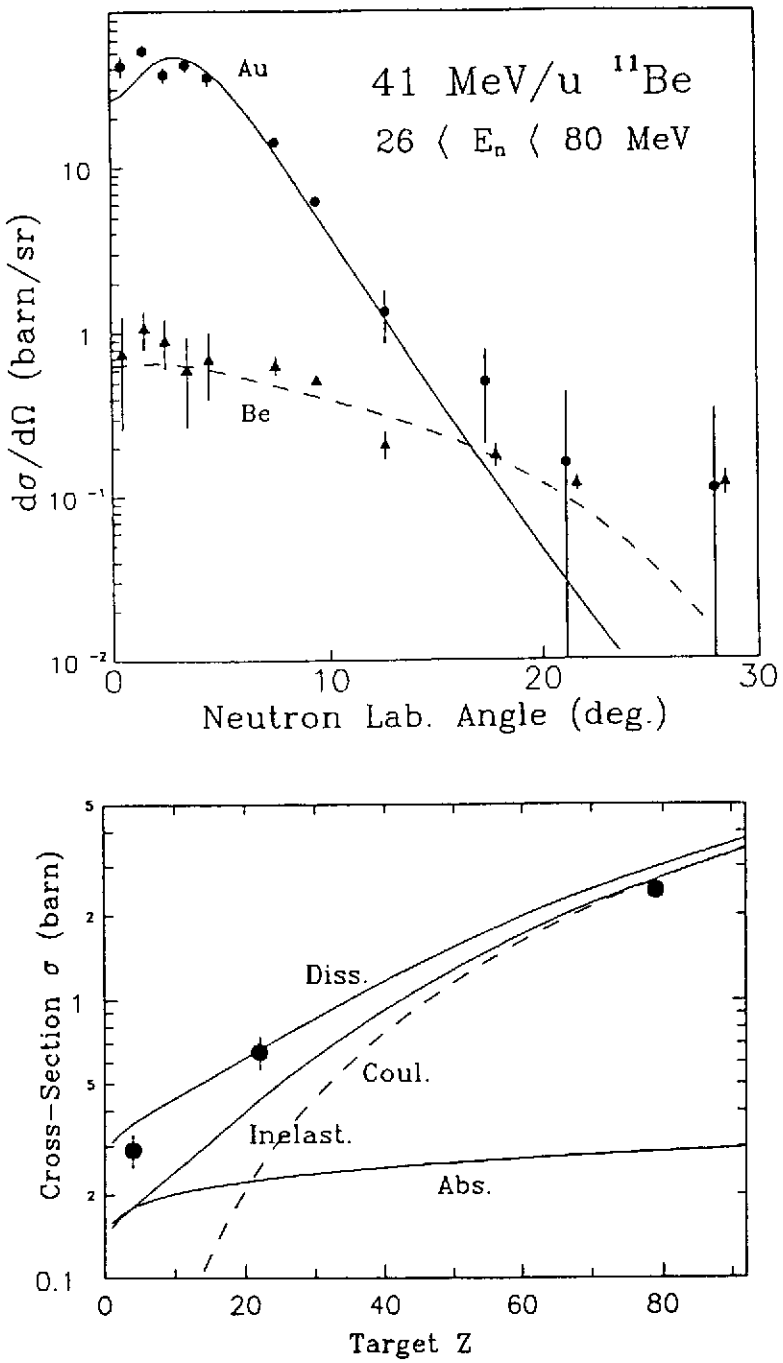

Figure 8: Upper panel: neutron angular distributions for the channel ^{10}Be + n following the breakup of a 41 MeV/nucleon ^{11}Be beam on Be and Au targets [21]. The calculated Coulomb and diffraction dissociation distributions for the Au and Be targets are indicated by the solid and dashed curves respectively. Lower panel: angle integrated cross sections for the same channel for Be, Ni and Au targets (points). The calculated Diss(ociation) cross section is decomposed into the Abs(orption) and Coul(omb) contributions. The line marked Inelast(ic) is the sum of both the Coulomb and diffraction dissociation contributions [22].

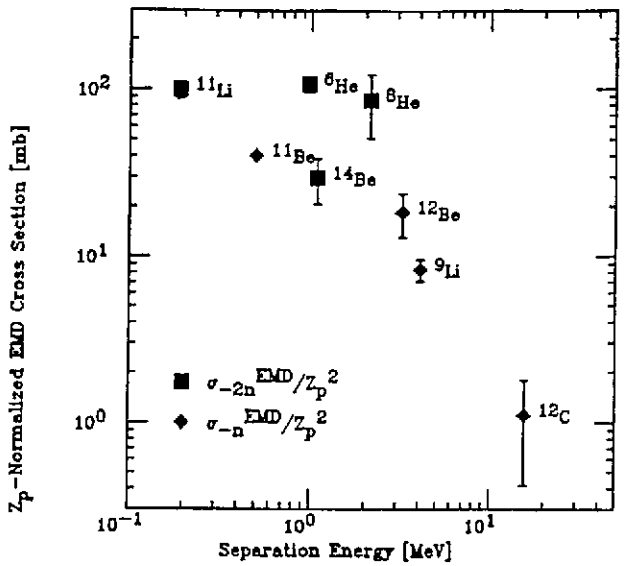

Figure 9: EMD cross sections as a function of binding energy of the valence neutrons for the dissociation of a number light nuclei [24].

confining effects of increasing angular momentum are well illustrated in figure 11, where a more realistic Woods-Saxon potential has been employed.

Using such potentials and including nonzero orbital angular momenta, as well as explicit treatment of the two-neutron halo, the general evolution of the development of halo structures with mass, binding and l (or the related hypermoment, K, for two-neutron haloes) has been explored by Fedorov *et al.* [27]. As a result some general scaling rules have been derived. In particular a limit of a few $MeV.A^{-2/3}$ on the separation energy, $S_{n/2n}$ has been estimated for the formation of a halo. As shown in figure 12, ^{6}He, ^{11}Li, ^{11}Be, ^{19}C and ^{19}B conform to these limits — ^{19}C being the subject of recent attention [29, 30], while ^{19}B is not yet experimentally accessible. The approximate nature of such a limit is apparent in the case of ^{14}Be, a known halo system (section II).

Before proceeding to the final section, the possibility of the existence of proton haloes must also be addressed. Considering only the binding energy and mass, two systems stand out: ^{8}B (S_p = 0.14 MeV) and ^{17}Ne (S_{2p} = 0.96 MeV). In the former case the valence proton has a predominantly $\pi p_{3/2}$ configuration, while for the latter a large (~50%) $\pi 2s^2_{1/2}$ admixture is predicted [31]. As the valence nucleon is charged, the behaviour of the wavefunction will also be affected by the Coulomb barrier,

$$U(r) = \frac{Z_{halo}Z_{core}e^2}{r} erf(\frac{r}{R}) \qquad (14)$$

Thus for systems with the same mass, valence nucleon binding energy and configuration, the charged matter distribution will be more confined than that for the neutrons (figure 11). Given the added confinement provided by the Coulomb barrier, it would appear difficult to form proton haloes of appreciable size for masses beyond $A \sim 20$. Experimentally the situation regarding ^{8}B has been somewhat unclear, with a number of contradictory claims being made. However recent measurements [32, 33, 34, 35] and theoretical work [16, 17] indicate that, while not as large as originally thought, ^8B does possess an extended valence

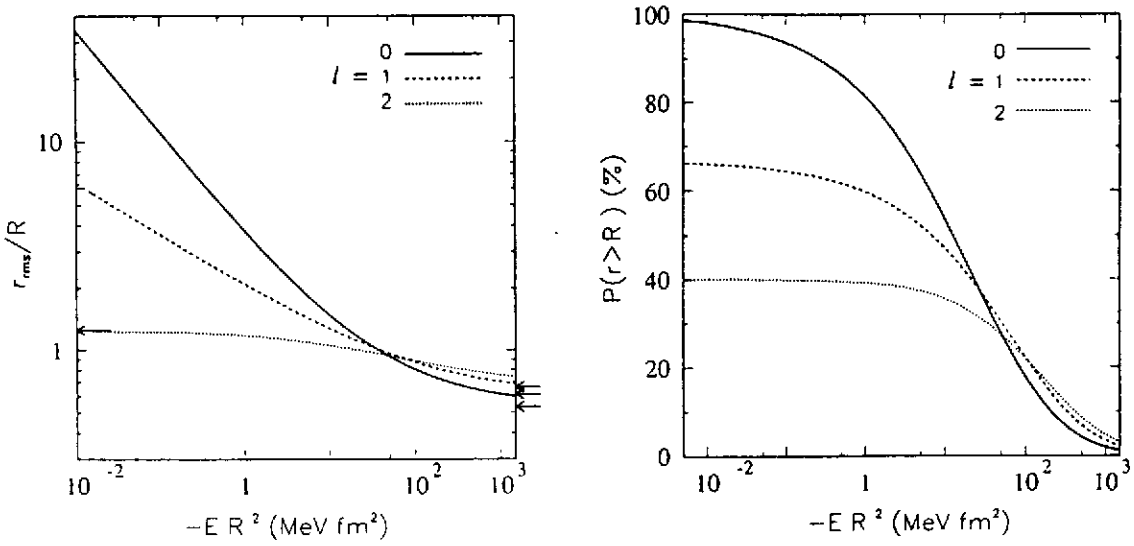

Figure 10: Left panel: RMS halo radius as a function of binding energy E and l. Right panel: Probabilty, P_l, of finding the valence neutron outside the square-well potential as a function of binding energy and l [26].

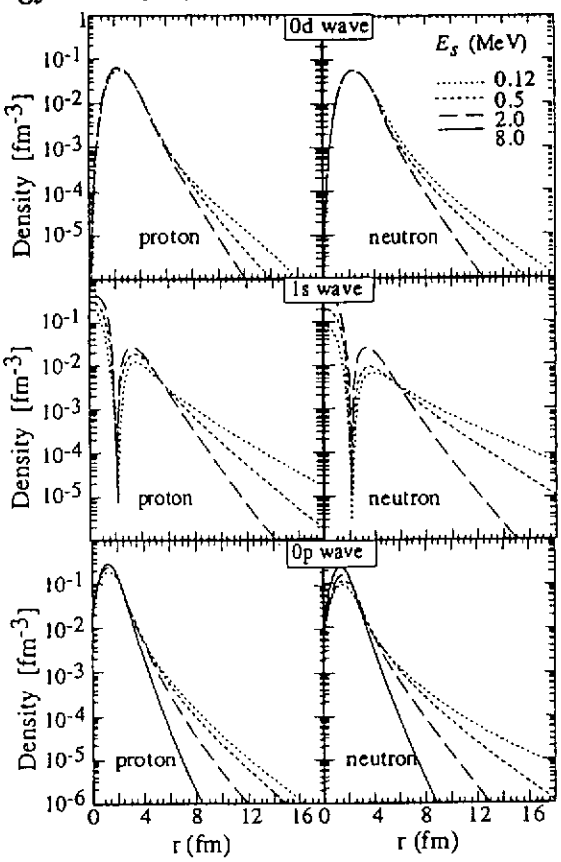

Figure 11: Single-particle density distributions ($A_c = 7$) as a function of valence nucleon binding energy, E_S, and configuration [25].

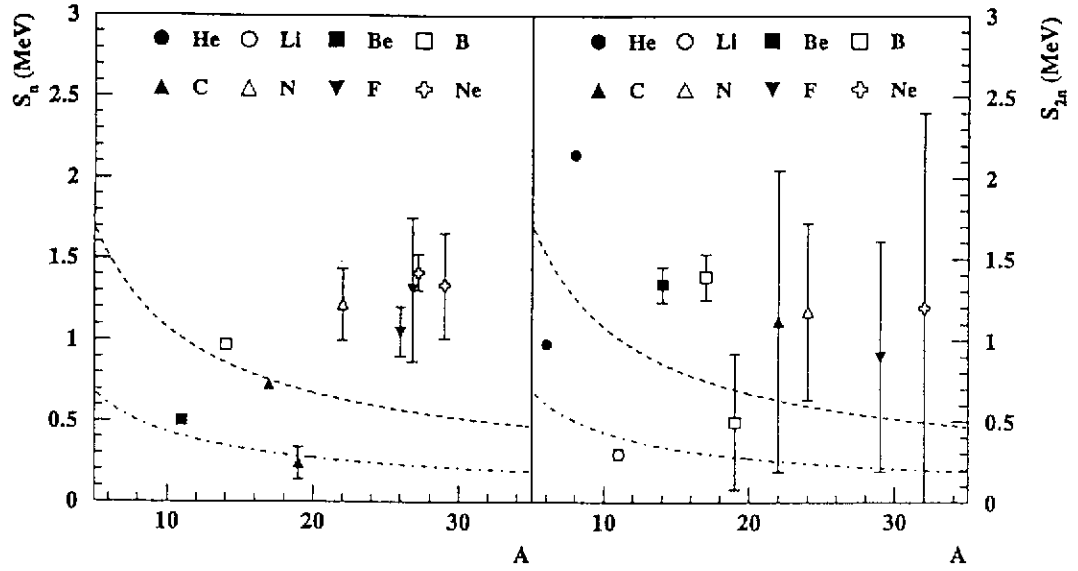

Figure 12: Separation energy, $S_{(2)n}$, versus mass for light, weakly bound, neutron-rich nuclei (from [28]). Dot-dashed line: $2.A^{-2/3}$MeV. Dashed line: $5.A^{-2/3}$MeV.

proton distribution. Work presently underway should shed light in the near future on ^{17}Ne [36].

IV Resonances and Correlations?

The very weak binding of the valence neutrons and the separation of the system into core and halo clusters has lead to the proposal of a new type of resonance in halo nuclei; namely the "Soft Dipole Resonance" or SDR [14, 37]. In normal nuclei, oscillations (or resonances) with a multipolarity of $\lambda = 1$ can be induced between the total neutron and total proton distributions[10] [2]. Such "Giant (Electric) Dipole Resonances" (GDR) have long been known and occur, owing to the relatively strong restoring force between the neutron and proton distributions, at excitation energies of $\sim 15 - 25$ MeV. Drawing an analogy with the GDR, E1 oscillations have been postulated to occur between the core and halo neutron distribution [37]. The low binding of the halo neutrons and consequent weak restoring force would be expected to drive such a resonance to low excitation energies ($\sim$ 1 MeV); hence the term "soft"[11].

As with the GDR, any soft-dipole mode should be preferentially excited via Coulomb excitation, with considerable enhancement expected for the E1 strength function, $dB(E1)/dE_x$, at low excitation energies. Owing to the very low binding the nucleus will, however, undergo dissociation into the core + halo neutrons. The enhanced low-lying E1 strength will thus translate into a large EMD dissociation cross section. As noted in section II, large cross sections are observed for reactions with high-Z targets — the decrease with increasing separation energy (figure 9) being inline with an increasing restoring force driving the resonance to higher excitation energies. Such high cross sections may, of course, be

[10] A more complete description is provided by the accompanying course of Philippe Chomaz.
[11] The conventional GDR would still be present at higher energies.

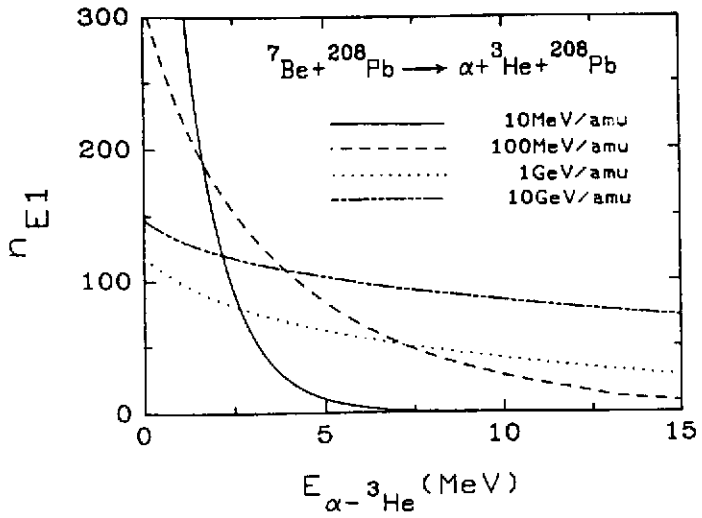

Figure 13: Example of the behaviour of the virtual photon spectrum with beam energy. In this case the n_{E1} spectrum is shown for ^{7}Be + ^{208}Pb [39].

simply associated with direct breakup to the continuum rather than via an intermediate resonance.

Experimentally the E1 strength function may be extracted from a measurement of the excitation spectrum from reactions on a high-Z target. Such reactions may be viewed as the absorption of a virtual photon, corresponding to the Coulomb field of the target. Importantly the form with excitation energy (E) of the virtual photon spectrum, $n_{E\lambda}$, depends on the beam energy [38] — at low energy the spectrum is dominated by low energy photons, while at higher beam energies the spectrum becomes flatter, and excitations to higher energies become possible (figure 13). The double differential cross section (σ_C) is, considering only dipole excitations [38],

$$\frac{d^2\sigma_C}{dEd\Omega} = \frac{dn_{E1}(E,\Omega)}{d\Omega}\frac{\sigma_{E1}(E)}{E} \tag{15}$$

where the dipole excitation cross section is given by,

$$\sigma_{E1} = \frac{16\pi^3}{9\hbar c}E\frac{dB(E1)}{dE} \tag{16}$$

Integrating over all trajectories, equation 15 becomes,

$$\frac{d\sigma_C}{dE} = \frac{n_{E1}(E)}{E}\sigma_{E1}(E) \tag{17}$$

Thus, the dipole strength function, $dB(E1)/dE$, may be derived from a measurement of the Coulomb excitation spectrum, $d\sigma_C/dE$.

As noted above, even relatively small excitations lead to the dissociation of halo nuclei. The experimental determination of $d\sigma_C/dE$ is thus challenging, requiring measurement of the momenta of the charged core and halo neutrons following the breakup of beams with intensities of only some $10^2 - 10^4$ pps. From such "kinematically complete" measurements the excitation energy in the nucleus prior to breakup may be reconstructed.

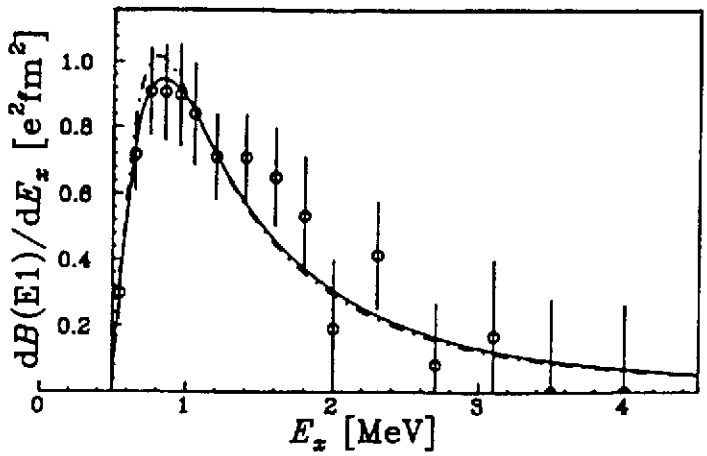

Figure 14: Dipole strength function for ^{11}Be, extracted from a measurement of breakup on Pb at 72 MeV/nucleon [40]. The solid line is the prediction for direct breakup.

An example is shown in figure 14 for the reaction of a ^{11}Be beam on a Pb target [40]. Here the E1 strength is seen to be concentrated at low energies, in line with expectations for an SDR. As the wavefunction is well known (section II), the dipole strength function may be calculated from first principles. Interestingly, the data is well reproduced assuming direct breakup. Further support for such non-resonant breakup is found in a comparison of the velocities of the core fragments (^{10}Be) and the neutrons, with that of the core being on average higher than than that of the neutrons. In simple terms, such a difference corresponds to the dissociation taking place around the distance of closest approach of the projectile and target, whereby only the charged core is subject to reaccelaration on the outgoing leg of the trajectory. In contrast, for a resonance, the dissociation would take place on average well after the point of closest approach, thus suppressing such a velocity difference.

In the case of ^{11}Li a number of experiments have been performed [41, 42, 43]. Similar enhancements in the low-lying E1 strength function are observed in all measurements at $E_x \sim 1$ MeV (figure 15), however the observation of a core-neutron velocity difference [41] and the form of the distribution [42] suggest that the breakup is, once again, direct.

In comparing the various measurements and theoretical predictions, two important constraints must be underlined. Firstly, as noted above, the virtual photon spectrum is heavily weighted towards low energies at the lower beam energies, thus biasing these experiments towards the population of low energy excitations. This effect is further compounded by the acceptances of the experimental setups, which decrease with increasing decay energy, E_d ($E_d = E_x - S_{(2)n}$). These two effects are clearly apparent in figure 15 (upper panel). It is important to note that the acceptance effects may only be calculated based on an assumed form for the excitation energy spectrum, thus precluding any model independant analysis.

Both effects may, however, be reduced by employing very high energy beams (>100 MeV/nucleon). At such energies, not only are higher excitations attainable through the increase in flux of high energy virtual photons, but the strong forward focussing of the

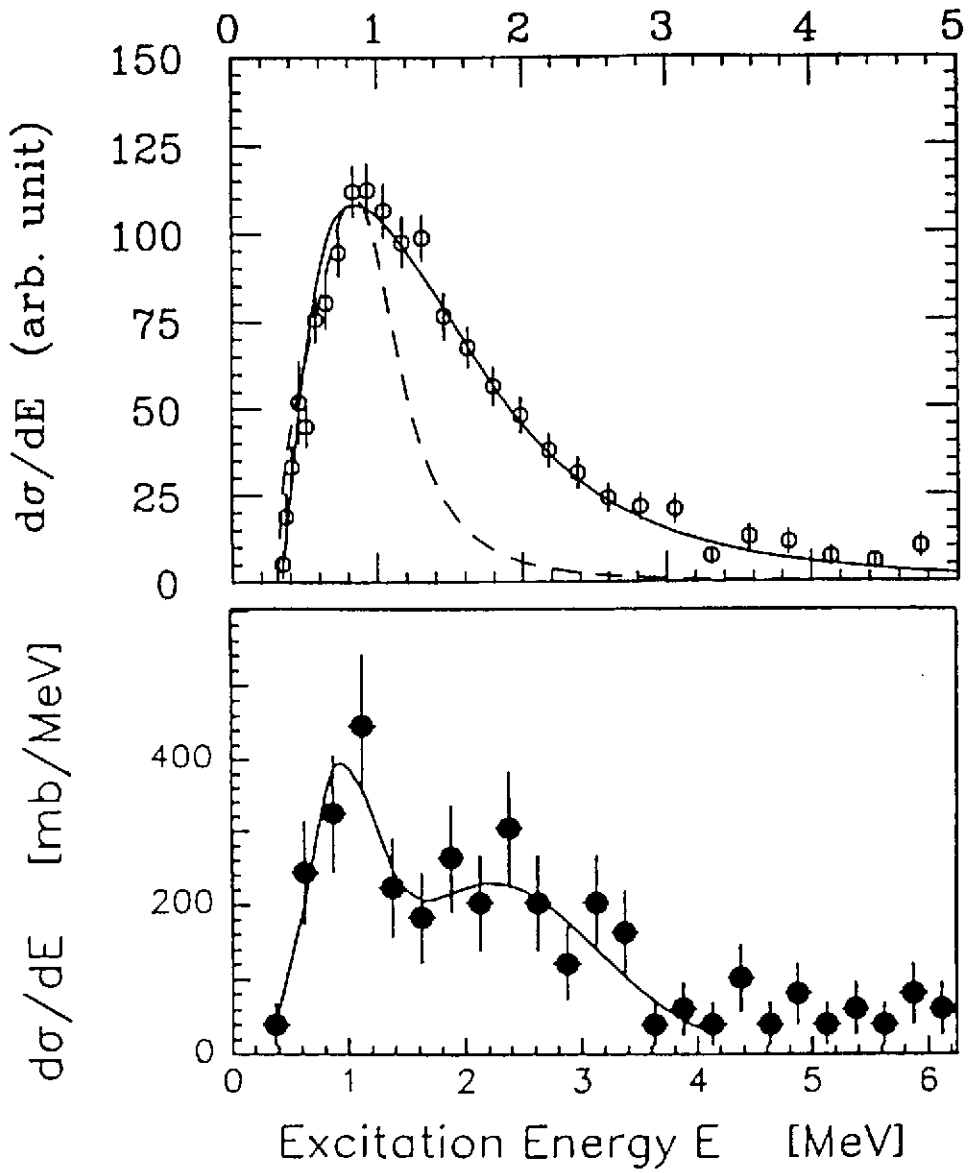

Figure 15: Invariant mass spectra for the breakup of ^{11}Li on Pb at 43 MeV/nucleon [42] (upper panel) and at 280 MeV/nucleon [43] (lower panel). The lineshape obtained at 28 MeV/nucleon [41] is included in the upper panel (dashed line) for comparison; note that the normalisation is arbitary and the uncertainties are not included. The solid line in the upper panel is a direct breakup prediction (see ref. [42] for details of the wavefunction used). The solid line in the lower panel is a two gaussian component fit to the data.

reaction products leads to 100% geometrical efficiencies. The results from the first experiment of this kind, carried out at GSI, is shown in figure 15 (lower panel), where additional strength is observed in the region of 2 MeV excitation energy.

The three-body nature of two-neutron halo systems represents one of the most intrinsically intriguing features of halo nuclei. As noted in section II, the simplest model reduces the description to a two-body system: core plus dineutron [14]. Inspired in part by this simple picture and the Borromean character[12] of two-neutron halo nuclei, the existence and nature of correlations between the halo neutrons has remained a central theme.

To study experimentally such correlations, processes must be sought in which the intrinsic neutron-neutron correlations are perturbed as little as possible. The avenue exploited to date has been dissociation reactions on high-Z targets. Here the relatively low energy excitations (described above) involved in the breakup are hoped to provoke only minimal perturbations in the intrinsic neutron-neutron momenta[13]. In principle then, in the kinematically complete experiments employed to map the E1 strength, the neutron-neutron relative momenta (p_{n-n}) may be extracted and used as a probe of correlations. Such measurements are experimentally difficult, owing primarily to the interferring effects of cross-talk, whereby neutrons may be scattered from one detector (or passive support material) into another, thus mimicking a two-neutron event or deforming the momentum of one neutron and hence the p_{n-n} [41, 45].

To date all three kinematically complete experiments on ^{11}Li [41, 42, 43, 44] have been used to reconstruct the p_{n-n} (eg., figure 16). Attempts have been made to compare the results with respect to the very simple pictures of strong spatial correlations or none whatsoever, with a strong dineutron like component appearing to be excluded [42, 43, 44]. The simplicity of the present analyses, which do not include, for example, the possibility of distortions from the reaction, must be stressed.

Ideally, the coupling of detailed theoretical calculations with measurements such as those described should provide a clearer picture of the neutron-neutron correlations and the low-lying E1 strength. Unfortunately, the incomplete description presently available for the ground state wavefunctions of ^{11}Li, ^{14}Be, etc remains a major obstacle, as does the need to correctly include the distorting effects of the reaction and FSI that govern the transformation of the ground state wavefunction to the observed excitation energy spectrum and neutron-neutron momentum distribution. In principle, ^{6}He provides a stepping stone in such studies owing to the well established nature of the $\alpha + n$ interaction (^{5}He). However, as outlined by Vaagen *et al.* [46], the understanding of such systems (in particular the continuum) is still far from complete.

V Conclusions and Perspectives

It is clear from the aforegoing discussion that many open questions remain regarding the halo. In general terms, while the conditions governing the development of haloes have

[12]None of the constituent two-body subsystems are bound.

[13]In this context experiments conducted at the lower energies may present an advantage.

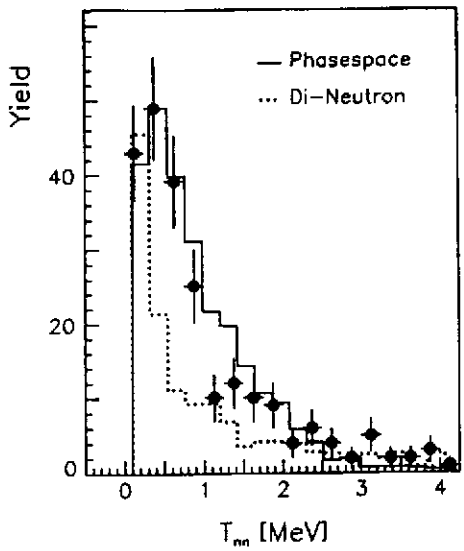

Figure 16: Neutron-neutron relative energy spectrum from the breakup of ^{11}Li on Pb [43]. Simulations taking into account the excitation energy spectrum (figure 15) and experimental detection efficiences are shown for dineutron (dotted line) and uncorrelated, or phasespace, emission (solid line). Both simulations have been arbitarily normalised to the data.

been addressed theoretically (section III), experimentally work has only just begun with excursions beyond the mass 11 systems (eg., ref's [29, 30]). While only briefly mentioned, similar remarks apply to proton haloes. Given that the halo is essentially a threshold phenomena, many more examples probably exist as excited states than ground states. Owing to the difficulties in gaining direct information regarding the size of an excited state[14], much remains to be done in this direction.

From a structural point of view, the spectroscopy of halo nuclei, including in the case of Borromean nuclei the related unbound systems (^{5}He, ^{10}Li, ^{13}Be), is vital. As noted, for example, in section III, the configuration of the valence nucleons influence directly the spatial extent of the system. On the theoretical side, few-body models have made considerable progress, with reasonable success obtained in reproducing the characteristics of well know systems such as ^{6}He. Steps have also been made towards more realistic modelling via the introduction of core degrees of freedom.

The excited state structure, and in particular putative SDR's, of halo nuclei remain, beyond the pioneering experiments described here largely unexplored. Additionally, while conceptually seductive, the investigation of correlations between halo nucleons remains in its infancy, with only the simplest of models being employed to compare with the scant experimental data. Theoretically much uncertainty remains in adressing both the SDR and correlations, stemming in part from the dearth of spectrocopic information and the complexity of including both realistic wavefunctions, reaction models and treatment of FSI.

It should be noted that space has not allowed the discussion of a number of experimental probes. For example, β-decay offers a potentially rich source of information via a well

[14]At present only γ-decay transition rates [47] and capture cross sections [48] can provide information on the radial extent of excited states.

understood mechanism [49]. Additionally, with the increasing intensities of secondary beams more conventional spectroscopic tools, such as direct reactions (eg. (p,p), (p,d), etc), are coming into play [50].

Perhaps the most appropriate note to end on is the following quotation which, it is hoped, captures the essence of the current situation in the field.

"These subjects were simple but not easy. So many zero order questions had to be answered in order to even make remote sense of what was going on. Such questions still exist, ..."

Denys Wilkinson

VI Further Reading

Beyond the articles cited in the text referring to particular experiments or models, a number of reviews exist.

For those interested in the more general question of nuclear sizes and density distributions, exhaustive treatments may be found in the text (theoretically orientated) by Barrett and Jackson [51] and, more recently, in a review of experimental probes by Batty *et al.* [52].

For a brief and lucid overview of halo states, the review by Karsten Riisager [12] is recommended. A more complete and detailed discussion may be found in the review prepared by Gregers Hansen, Axel Jensen and Björn Jonson [53], while many of the experimental aspects of halo studies are included in a recently compiled review by Isao Tanihata [25]. A comprehensive, if slightly less up-to-date, compilation of theoretical models — concentrating in particular on three-body descriptions of Borromean systems — is provided by the reviewed prepared by the RNBT collaboration [54].

Bibliography

[1] R Hofstadter, Ann. Rev. Nucl. Sci. **7** (1957) 231

[2] A Bohr, B Mottelson, *Nuclear Structure*, WA Benjamin, New York (1969)

[3] MH Johnson, E Teller, Phys. Rev. **93** (1954) 357

[4] JA Nolen Jr., JP Schiffer, Ann. Rev. Nucl. Sci. **19** (1969) 471

[5] P Van Duppen, *"Les Noyaux Exotiques"*, lecture notes to this School

[6] I Tanihata *et al.*, Phys. Rev. Lett. **55** (1985) 2676; Phys. Lett. **106B** (1985) 380; Phys. Lett. **B206** (1988) 592

[7] E Arnould *et al.*, Phys. Lett. **B197** (1987) 311

[8] B Blank *et al.*, Z. Phys. **A343** (1992) 375

[9] Y Ogawa *et al.*, Nucl. Phys. **A543** (1992) 722

[10] GD Alkhazov *et al.*, Phys. Rev. Lett. **78** (1997) 2313

[11] JS Al-Khalili, JA Tostevin, Phys. Rev. Lett. **76** (1996) 3903

[12] K Riisager, Rev. Mod. Phys. **66** (1994) 1105

[13] H Sagawa, Phys. Lett. **B286** (1992) 7

[14] PG Hansen, B Jonson, Europhys. Lett. 4 (1987) 409

[15] NA Orr, Nucl. Phys. **A616** (1997) 155c

[16] PG Hansen, Phys. Rev. Lett. **77** (1996) 1016

[17] H Esbensen, Phys. Rev. **C53** (1996) 2007; K Hencken *et al.*, Phys. Rev. **C54** (1996) 3043

[18] J Hüfner, MC Nemes, Phys. Rev. **C23** (1981) 2538

[19] R Serber, Phys. Rev. **72** (1947) 1008

[20] JH Kelley *et al.*, Phys. Rev. Lett. **74** (1995) 30

[21] R Anne *et al.*, Phys. Lett. **B304** (1993) 55

[22] R Anne *et al.*, Nucl. Phys. **A575** (1994) 125

[23] F Nunes *et al.*, Nucl. Phys. **A596** (1996) 171

[24] T Kobayashi, *Proc. 1st Int. Conf. on Radioactive Nuclear Beams*, Sept. 1989, Berkeley, USA, ed. WD Myers, JM Nitscke, EB Norman (World Scientific, 1990) p325

[25] I Tanihata, J. Phys. G: Nucl. Part. Phys. **22** (1996) 157

[26] K Riisager, AS Jensen, P Moller, Nucl. Phys. **A548** (1992) 393

[27] DV Fedorov, AS Jensen, K Rissager, Phys. Lett. **B312** (1993) 1; Phys. Rev. **C49** (1994) 201

[28] E Liegard, Thèse, Université de Caen (1998)

[29] D Bazin *et al.*, Phys. Rev. Lett. **74** (1995) 3569

[30] FM Marqués *et al.*, Phys. Lett. **B381** (1996) 407

[31] NK Timofeyuk *et al.*, Nucl. Phys. **600** (1996) 1

[32] W Schwab *et al.*, Z. Phys. **A350** (1995) 283

[33] JH Kelley *et al.*, Phys. Rev. Lett. **77** (1996) 5020

[34] F Negoita *et al.*, Phys. Rev. **C54** (1996) 1787

[35] B Blank *et al.*, Nucl. Phys. **A624** (1997) 242

[36] A Ozawa *et al.*, Phys. Lett. **B334** (1994) 18

[37] K Ikeda, Nucl. Phys. **A538** (1992) 355c

[38] CA Bertulani, G Baur, Phys. Rep. **163** (1988) 299

[39] G Baur *et al.*, Nucl. Phys. **A458** (1986) 188

[40] T Nakamura *et al.*, Phys. Lett. **B331** (1994) 296

[41] D Sackett *et al.*, Phys. Rev. **C48** (1993) 118; K Ieki *et al.*, Phys. Rev. Lett. **70** (1993) 730

[42] S. Shimora *et al.*, Phys. Lett. **B348** (1995) 29

[43] M Zinser *et al.*, Nucl. Phys. **A619** (1997) 151

[44] K Ieki *et al.*, Phys. Rev. **C54** (1996) 1589

[45] Z Wang *et al.*, Nucl. Instr. Method **A397** (1997) 380

[46] J Vaagen *et al.*, Nucl. Phys. **A616** (1997) 426

[47] MJG Borge *et al.*, Phys. Lett. **B317** (1993) 25

[48] T Otsuka *et al.*, Phys. Rev. **C49** (1994) R2289

[49] K Riisager, Nucl. Phys. **A616** (1997) 169

[50] JS Winfield *et al.*, Nucl. Instr. meth. **A396** (1997) 147

[51] RC Barrett, DF Jackson, *Nuclear Sizes and Structure*, Clarendon Press, Oxford (1979)

[52] CJ Batty *et al.*, Advances Nucl. Phys. **19** (1989) 1

[53] PG Hansen, AS Jensen, B Jonson, Ann. Rev. Nucl. Part. Sci **45** (1995) 591

[54] MV Zhukov *et al.*, Phys. Rep. **231** (1993) 151